# Effects of electron irradiation on graphene drums FREE

Ibikunle Ojo 💿 ; Evan Hathaway; Jianchao Li; Roberto Gonzalez 💿 ; Yan Jiang; Jingbiao Cui; Jose Perez 💿



J. Vac. Sci. Technol. A 42, 012201 (2024) https://doi.org/10.1116/6.0003159





CrossMark

■ Knowledge
■ Expertise
Click to view our product catalogue
Contact Hiden Analytical for further details

② www.HidenAnalytical.com
② info@hiden.co.uk

■ Contact Hiden Analytical for further details
■ Contact Hid



# Effects of electron irradiation on graphene drums

Cite as: J. Vac. Sci. Technol. A 42, 012201 (2024); doi: 10.1116/6.0003159 Submitted: 21 September 2023 · Accepted: 14 November 2023 · Published Online: 22 December 2023







Ibikunle Ojo,¹ 📵 Evan Hathaway,¹ Jianchao Li,² Roberto Gonzalez,¹ 📵 Yan Jiang,¹ Jingbiao Cui,¹ and Jose Perez<sup>1,a)</sup>

#### **AFFILIATIONS**

- Department of Physics, University of North Texas, Denton, Texas 76203
- <sup>2</sup>Materials Research Facility, VP Research and Innovation Office, University of North Texas, Denton, Texas 76203
- a)Electronic mail: jose.perez@unt.edu

#### **ABSTRACT**

Using a scanning electron microscope, we irradiate graphene drums with electrons at an energy of 20 keV and a dosage of about  $1.58 \times 10^{17}$  electrons/cm<sup>2</sup>. The drums consist of graphene exfoliated in ambient air over holes having a diameter of  $4.6 \,\mu m$  and etched into an SiO<sub>2</sub> substrate. After irradiation, we observe that the drum's suspended monolayer (ML) region has a ratio of the Raman D peak height, an SiO<sub>2</sub> substract. Then  $I_D$ , to the Raman G peak height,  $I_G$ , as high as 6.3. In contrast, the  $I_D$  to the Raman G peak height,  $I_G$ , as high as 6.3. In contrast, the  $I_D$  studies have shown that graphene drums containing air can leak in a vacuum at a low rate. We attribute the  $I_D$  pended ML to the air that may be in the drums. We propose that the air produces much adsorbed water on the ML, resulting in a high average defect density during irradiation. We present Raman maps of the full-width-at-half maximum, position, and height of the G,  $I_D$ , and  $I_D$  peaks before and after irradiation and maps of  $I_D/I_G$  and  $I_D/I_D$ . We anneal the drums at temperatures from 50 to 215 °C and find that  $I_D/I_G$  significantly reduces to 0.42. The annealing data are analyzed using an Arrhenius plot. We also find that  $I_D/I_D$  depends on annealing temperature and has values  $\geq 8$ , in the range expected for  $I_D/I_G \leq 3.9$ . This irradiation method may help achieve  $I_D/I_D \leq I_D/I_D$  depends on annealing temperature and has values  $\geq 8$ , in the range expected for  $I_D/I_G \leq 3.9$ . This irradiation method may help achieve  $I_D/I_D \leq I_D/I_D$  depends on annealing temperature and has values  $I_D/I_D$  depends on  $I_D/I_D$  dep

# I. INTRODUCTION

This paper reports the irradiation of graphene drums using a scanning electron microscope (SEM) at an electron beam energy of 20 keV to a dosage of about  $1.58 \times 10^{17}$  electrons/cm<sup>2</sup>. Such irradiation results in a ratio of the Raman D peak height,  $I_D$ , to G peak height,  $I_G$ , which is significantly higher than that reported using graphene supported on solid SiO<sub>2</sub>/Si substrates. 1-10 Since graphene's  $I_D/I_G$  ratio measures the average defect density, this technique may help produce defects at higher average densities. The graphene drums consist of graphene mechanically exfoliated over micrometer-size holes in SiO2/Si substrates under ambient air at atmospheric pressure and room temperature (RT). After irradiation, the  $I_D/I_G$  ratio of monolayer (ML) graphene regions in drums is as high as 6.3 at a laser wavelength of 532 nm, significantly higher than the maximum  $I_D/I_G$  value of about 3.3 at a laser wavelength of 514 or 532 nm reported for supported ML graphene after electron irradiation using an SEM,<sup>1-6</sup> exposure to a hydrogen plasma, and bombardment with Ar ions. Previous studies have reported that graphene drums containing an atmosphere of air can leak air in a vacuum at a low rate. 11 We attribute the high  $I_D/I_G$ 

ratio to air that may be inside the drums. We obtain spatial maps of the characteristics of the Raman G, 2D, D, and D' peaks, such as the full-width-at-half maximum (FWHM), position, and height for graphene drums before and after irradiation and present corresponding maps of  $I_D/I_G$  and  $I_D/I_{D'}$ , where  $I_{D'}$  is the height of the D'peak. We thermally anneal the irradiated drum to 215 °C, and study the behavior of  $I_D/I_G$  and  $I_D/I_{D'}$  with annealing temperature.

The D peak in graphene, which occurs at about  $1330 \,\mathrm{cm}^{-1}$ , is due to a breathing mode of the carbon rings and is not active in perfect crystals but becomes active when defects are present.<sup>12</sup> The D peak active regions are nanocrystalline regions having diameters of a few nanometers that surround each defect on the graphene. In samples where a defect may occur with equal probability anywhere on its surface, n, the number of D peak active regions and  $I_D$ increase with n at sufficiently low defect densities. In contrast, the G peak, which occurs at about 1580 cm<sup>-1</sup>, is due to the opposing motion of adjacent carbon atoms, and its height is independent of n. Therefore,  $I_D/I_G$  measures n without dependence on the incident laser power. For the case of graphene bombarded with Ar ions, the  $I_D/I_G$  ratio exhibits a first stage in which it increases with ion

dosage and then, after reaching a maximum, transitions to a second stage in which it decreases with dosage.<sup>8–10</sup> The defects, in the case of Ar ion bombardment, are vacancies. The model that explains this behavior states that the defects and active nanocrystalline regions do not overlap in the first stage, so  $I_D/I_G$  increases with n. However, n is so high in the second stage that defects overlap, resulting in the entire lattice becoming defective and losing its D peak active regions. The sample becomes amorphous in the second stage due to the high density of vacancies. The model predicts that in the first stage,  $n \propto I_D/I_G$ , while in the second stage,  $n \propto 1/(I_D/I_G)$ . The maximum value of  $I_D/I_G$ , which depends on the excitation laser wavelength, occurs at the transition between the first and second stages.

The effects of electron irradiation on ML graphene at electron energies of 5-30 keV using an SEM have been extensively reported due to the prevalence of this technique in imaging and lithography.<sup>1-3</sup> Although such electron energies are below the threshold of about 80 keV for electrons to cause knock-on displacement of C atoms, 13,14 the irradiation produces a D peak, and  $I_D/I_G$  displays a two-stage behavior similar to the case of Ar ion bombardment. Therefore, the graphene appears to follow a path of irreversible amorphization. However, authors also report that SEM irradiation at these energies can reversibly modify graphene, imparting novel and potentially valuable properties. For example, electron irradiation can hydrogenate<sup>6</sup> and dope<sup>15</sup> graphene, produce sp<sup>3</sup>-type defects in graphene, thange the electrical transport of fluorinated graphene, 16 and produce magnetic regions in hydrogenated graphene.<sup>17</sup> In Ref. 6 the hydrogenation was accomplished by coating the ML graphene with hydrogen silsesquioxane (HSQ); the mechanism was thought to be electron-induced dissociation of hydrogen from HSQ. We have previously reported evidence that electron irradiation at 30 keV of ML graphene with adsorbed H<sub>2</sub>O and NH<sub>3</sub> produces hydrogenation. <sup>18</sup> In these experiments, we heated the graphene in an ultrahigh vacuum (UHV) chamber at about 590° C to remove adsorbates, exposed the graphene to gases, and irradiated it in situ in UHV. We saw a D peak after exposing the graphene to H<sub>2</sub>O and NH<sub>3</sub>, polar molecules that adsorb on graphene, but not after exposure to H2, Ar, CO2, or O2 gases. We concluded that the D peak was due to hydrogenation based on its occurrence only after exposure to the hydrogen-containing polar gases H<sub>2</sub>O and NH<sub>3</sub> and a significant decrease in  $I_D/I_G$  after annealing at 250 °C. We proposed the mechanism was electron-induced dissociation of hydrogen from adsorbed H<sub>2</sub>O and NH<sub>3</sub>.1

The leakage of gases in graphene drums has been extensively studied. 11,19-21 In drums consisting of graphene completely covering a hole, the leakage rates can be low, with most leakage occurring around the hole's edge. The low leakage rates are attributed to the impermeability of graphene to gases<sup>23</sup> and the extreme flexibility of graphene, resulting in a liquidlike seal between the graphene and substrate.<sup>24</sup> Various studies have utilized graphene drums in micromechanical applications. 25-28 To our knowledge, there have been no reports on the effects of electron irradiation on graphene drums. As the gas pressure increases, the density of adsorbed molecules on the surface typically increases, so if adsorbates are the source of defects during electron irradiation, performing irradiation experiments on graphene drums may increase the defect density. One method of investigating the effects

of irradiation at increased gas pressure is to use an environmental SEM (ESEM).<sup>29</sup> However, the maximum operating pressure in a commercial ESEM is limited to about 20 Torr due to beam spread at high pressures and the need to keep a low pressure in the column. The pressure the graphene drum can withstand before breaking would be the maximum pressure during irradiation. This pressure has been reported to be a few atmospheres.

# II. EXPERIMENT

Under atmospheric pressure, RT, and relative humidity of about 40%, we mechanically exfoliate graphene from highly oriented-pyrolytic graphite using the Scotch tape method onto an SiO<sub>2</sub>/Si substrate with a 350 nm thick SiO<sub>2</sub> layer that has holes etched into it. We employ photolithography and reactive ion etching (RIE) techniques to create these holes, which are approximately  $4.6\,\mu\mathrm{m}$  in diameter and  $500\,\mathrm{nm}$  in depth, with centers aligned in a square pattern and  $25 \,\mu m$  apart. We kept the substrates under ambient relative humidity conditions of about 40% before and after exfoliation. The graphene is irradiated using a JEOL JSM-7001F field emission SEM at an electron energy of 20 keV, a beam current of 0.29 nA, and vacuum of about 10<sup>-6</sup> Torr. We irradiate to a total electron dosage of  $1.58 \times 10^{17} \,\mathrm{e^{-/cm^2}}$  by continuously exposing an area of approximately  $56 \times 37 \,\mu\text{m}^2$  to the beam for 30 min. We chose this dosage because we have previously shown that it gives an n in supported ML graphene such that the Dpeak active areas are in the first stage of defect formation.<sup>5</sup> We measure the Raman spectra using a Renishaw inVia Raman microscope with a 532 nm laser, 1800 lines/mm grating, and an  $\times 100^{\circ}$  objective with a 0.76 um spot size. The laser power is 0.25 mW, and the acquisition time for spectra is 10 s. We use the Renishaw Wire 5.2 software to acquire the maps; spectra are measured at each point on a grid and fitted to obtain the FWHM, position, and second to obtain the fitted to o height of the peaks. For thermal annealing studies, the irradiated  $\frac{2}{5}$  graphene samples are heated in nitrogen gas at a flow rate of  $\frac{2}{5}$ 50 sccm for 5 min and at temperatures from 50 to 215 °C.

# **III. RESULTS AND DISCUSSION**

Figures 1(a)-1(d) show images of an exfoliated flake having ML and multilayer regions lying across two holes labeled 1 and 2. As discussed below, the "o's" in Fig. 1(b) denote the approximate locations where the Raman spectra in Fig. 2 were acquired. Figures 1(c) and 1(d) show SEM images of the flake. The flake covers Hole 1 entirely by a wide margin around the perimeter. We refer to the flake-Hole 1 structure as a completely covered drum. However, the flake appears to cover Hole 2 by a slim margin, as shown in Fig. 1(d). The red arrows in Figs. 1(c) and 1(d) show a channel unintentionally etched into the SiO<sub>2</sub> during the RIE process that connects the inside of Hole 2 with the exterior. We refer to this structure as a partially covered drum.

In Ref. 11, the authors reported that considering the air within the drum as an ideal gas, the leakage rate is approximately  $2 \times 10^3$  atoms/s. In our drum configuration, the perimeters of the holes are slightly smaller than those in Ref. 11, potentially resulting in less leakage. Assuming our completely covered drums seal the air inside with the same leakage rate as those in Ref. 11, an estimated  $7.2 \times 10^6$  atoms will escape from the drums per hour under



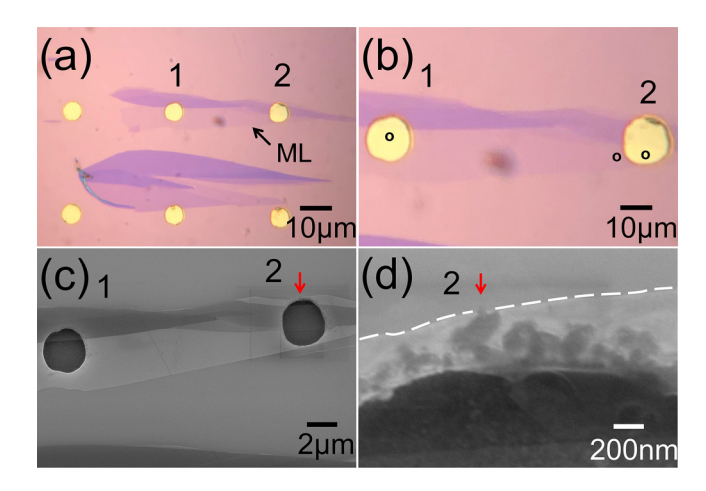


FIG. 1. Images of graphene drums. (a) Optical image of completely covered drum 1 and partially covered drum 2 containing ML graphene. (b) "o's" denote where Raman spectra were obtained. (c) and (d) SEM images with arrows indicating a channel etched into the substrate.

vacuum conditions. We have not proven that our completely covered drums seal the air inside, but we propose this to explain the high  $I_D/I_G$  ratios. Since the air density is approximately  $2.7 \times 10^{19}$  molecules/cm<sup>3</sup> at atmospheric pressure and RT, a drum in our substrate initially holds around  $1.7 \times 10^8$  molecules before SEM placement. The drum's total time in an SEM under vacuum is less than an hour. After an hour in a vacuum, the molecular count within the drum would decrease to  $2.3 \times 10^8 - 7.2 \times 10^6$ , equating to roughly  $2.2 \times 10^8$ , only a 4% decline. Under these assumptions, the pressure inside the drum after an hour in a vacuum would be approximately 0.96 atmospheres.

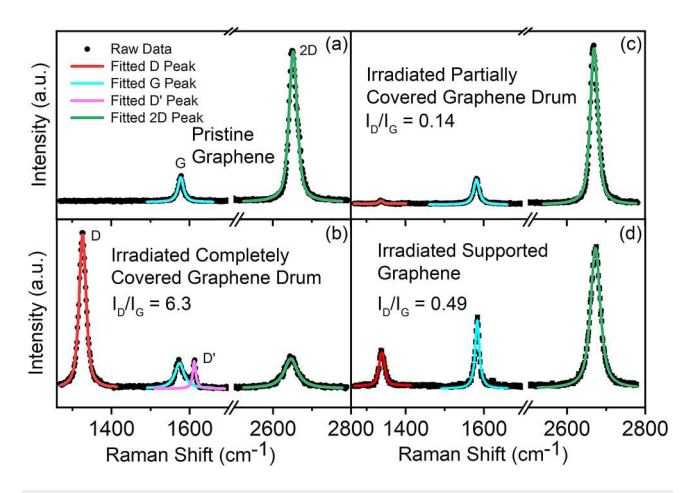


FIG. 2. Raman spectra obtained at the location of the "o's" in Fig. 1 with fits of the G, 2D, D, and D' peaks. (a) and (b) On the suspended ML over drum 1 before and after irradiation, respectively. (c) On the suspended ML over drum 2 after irradiation. (d) On the supported ML next to drum 2 after irradiation.

We obtain Raman maps of the completely covered drum before and after irradiation and the partially covered drum after irradiation. The maps were acquired the same day as the irradiation was done. Figures 2(a)-2(d) show representative Raman spectra from the maps taken near the locations denoted by "o" in Fig. 1(b). Shown are the fitted curves produced by the Wire 5.2 software. Figure 2(a) shows that the ML graphene over the completely covered drum does not display an observable D peak before irradiation. Figure 2(b) shows this ML has an  $I_D/I_G$  ratio of 6.3 after irradiation.

Figure 2(c) shows that the ML over the partially covered drum after irradiation has an  $I_D/I_G$  ratio of only 0.14. We attribute the completely covered drum's high  $I_D/I_G$  ratio to the assumed air sealed within the drum. As previously discussed, using the leakage rate reported In Ref. 11, there may be approximately one air atmosphere in the drum. The air atmosphere would produce a high density of adsorbed water on the graphene. We attribute the partially covered drum's significantly lower  $I_D/I_G$  ratio to the drum containing less air due to air evacuating through the edge of the hole or channels shown in Fig. 1(d) when the sample is in a vacuum. The lower air pressure would produce a lower adsorbed water density on the ML. Figure 2(d) shows that the supported ML next to the partially covered drum shows an  $I_D/I_G$  ratio of 0.49 following irradiation. We have previously attributed the  $I_D/I_G$  ratio after irradiation in supported MLs to water adsorbed on top of the ML or trapped between the ML and the SiO<sub>2</sub> substrate. 15 Therefore, we attribute the lower value of  $I_D/I_G$  of 0.14 for the ML suspended over the partially covered hole to fewer adsorbed water molecules on the top or bottom of the ML.

The results described above are reproducible. Table I shows the  $I_D/I_G$  and  $I_D/I_{D'}$  ratios of the sample discussed above (Sample #1) and three other samples (Samples #2-4) exfoliated on different substrates using the same procedure. The irradiation dosages for Samples #2-4 were 1.0, 5.0, and  $1.9 \times 10^{15}$  electrons/cm<sup>2</sup> to ensure  $\frac{15}{50}$ that the samples were in the first stage of defect formation. The Raman spectra and optical and SEM images of the additional samples are shown in the supplementary material.<sup>38</sup> The Raman spectra were averaged over three points shown in Figs. S1-S3 in the supplementary material<sup>38</sup> for the additional samples. As shown in Table I, in Samples #1-4, the  $I_D/I_G$  ratios of the suspended MLs over completely covered holes are 6.30, 5.28, 4.72, and 4.22, respectively, significantly higher than the maximum of 3.3 reported in the

**TABLE I.**  $I_D/I_G$  and  $I_D/I_{D'}$  ratios for ML regions of completely covered graphene drums, partially covered graphene drums, and graphene supported on the SiO2 substrate. The lower bound >14 for  $I_D/I_D$  for the supported ML in Sample #3 was estimated from the noise level, as discussed in Fig. S2 in the supplementary material.

	Completely covered		Partially covered		Supported	
Sample #	$I_D/I_G$	$I_D/I_D$	$I_D/I_G$	$I_D/I_D$ ,	$I_D/I_G$	$I_D/I_D$
1	6.30	6.87	0.14	N/A	0.49	8.17
2	5.28	8.44	0.16	N/A	0.48	9.20
3	4.72	9.37	0.14	N/A	0.20	>14
4	4.22	6.65	N/A	N/A	0.68	10.01

literature for supported MLs. Fig. S3 in the supplementary material shows that Sample #4 does not have an ML suspended over a partially covered hole. Samples #1–3 have MLs over partially covered holes, and their  $I_D/I_G$  ratios are 0.14, 0.16, and 0.14, respectively, significantly less than those for MLs over completely covered holes. The supported MLs in Samples #1–4 have  $I_D/I_G$  ratios of 0.49, 0.48, 0.20, and 0.68, respectively, significantly lower than those for the MLs over completely covered holes and greater than those for the MLs over partially covered holes.

Figure 3 illustrates our model. We assume that the adsorbed water molecules form thin layers on the ML graphene due to hydrogen bonding between the water molecules. 30,31 Only ML regions covered by water layers can become defective during irradiation. The mechanism is the dissociation of H2O by incident electrons, as previously reported.<sup>18</sup> In Fig. 3(a), there is less adsorbed water on the ML than in Fig. 3(b), so the ML in Fig. 3(a) will have a lower average value of  $I_D/I_G$  after irradiation. Our model explains that the  $I_D/I_G$  ratio variation between samples after irradiation is due to variations in the average adsorbed water density. In the case of Ar ion bombardment, the entire graphene lattice is equally likely to become defective since the ions interact directly with the C atoms. In Refs. 8–10, the maximum value of  $I_D/I_G$  for point defects, such as vacancies due to Ar ion bombardment, is about 2-3 at a laser wavelength of 514 or 532 nm. We believe the significantly higher value of  $I_D/I_G$  in completely covered drums may be due to the defects being different from vacancies, like sp<sup>3</sup> defects.

In our model, the  $I_D/I_G$  ratio of a probed sample area is an average that is proportional to the percentage of area covered by water layers, W, before irradiation and the defect density, n, in the regions covered by water layers during irradiation, i.e.,  $I_D/I_G \propto Wn$ . By average defect density, we mean  $n_{\rm avg} = Wn$ . We assume that the water density in the water layers and the probability of an incident electron dissociating a water molecule and producing a defect are the same for suspended and supported MLs. Consequently, the defect density, n, in regions covered by water layers during irradiation is the same in suspended and supported MLs. The suspended MLs have a greater  $I_D/I_G$  because the percentage of area covered by

water layers, W, is greater. Under these assumptions,  $(I_D/I_G)_{sus}/(I_D/I_G)_{sus}$  $I_G$ )<sub>sup</sub> =  $W_{sus}/W_{sup}$ , where  $(I_D/I_G)_{sus}$  and  $(I_D/I_G)_{sup}$  are the  $I_D/I_G$ ratios of the supported and suspended MLs, respectively, and  $W_{\rm sus}$ and  $W_{\text{sup}}$  are the percentage of area covered by water layers in the suspended and supported MLs, respectively. For Sample #1, we have  $W_{\text{sus}}/W_{\text{sup}} = 6.30/0.49 = 12.8$ ; thus, the suspended ML has about 13 times more defective area than the supported ML. Determining the defect density, n, in the defective areas covered by water layers during irradiation requires a model for how  $I_D/I_G$  in the defective areas varies with electron irradiation dosage,  $D_e$ . In Refs. 8-10, the authors give a model and equation for how  $I_D/I_G$ varies with the average distance between defects,  $L_D$ . In Ref. 5, we used this equation to fit  $I_D/I_G$  versus  $D_e$  for a supported ML sample and obtained, for this sample, the expression  $L_D = 100/\sqrt{D_e}$ , with  $L_D$  in nm and  $D_e$  in electrons/nm<sup>2</sup>. One of the experimental data points for the fit was  $I_D/I_G = 0.56$  at  $D_e = 1.44 \times 10^{17}$  electrons/cm<sup>2</sup>. This point is close to the values for the supported ML in Sample #1, which has  $I_D/I_G = 0.49$  at  $D_e = 1.58 \times 10^{17}$  electrons/cm<sup>2</sup>, so we use the expression  $L_D = 100/\sqrt{D_e}$  for Sample #1 to obtain an approximate value of  $L_D = 2.5 \text{ nm}$  and a defect density  $n = 1/L_D^2 = 1.6 \times 10^{13}/\text{cm}^2$  in the defective areas, which is about one defect per 240 carbon atoms.

Figures 4(a)-4(f) show maps of the G and 2D peaks for the completely covered drum before irradiation. The step size is  $0.5\,\mu\text{m}$ . In all the maps in this paper, the dashed circle denotes the approximate boundary between the hole and  $SiO_2$  substrate, and the dashed line marks the boundary between the ML and multilayer regions. The suspended area is inside the circle. The supported area is outside the circle and enclosed by the scanned area. In Fig. 4, the ML region is below the dashed line, and the multilayer region is above. The maximum and minimum of the scale bar for each map are set to the maximum and minimum of the data to produce the most color variation. We obtain average values of the FWHM, position, and height of the peaks in the suspended and supported areas by averaging over points excluding the boundaries. Any square with a boundary line going through is not counted in the average. All of the results for the completely covered drum

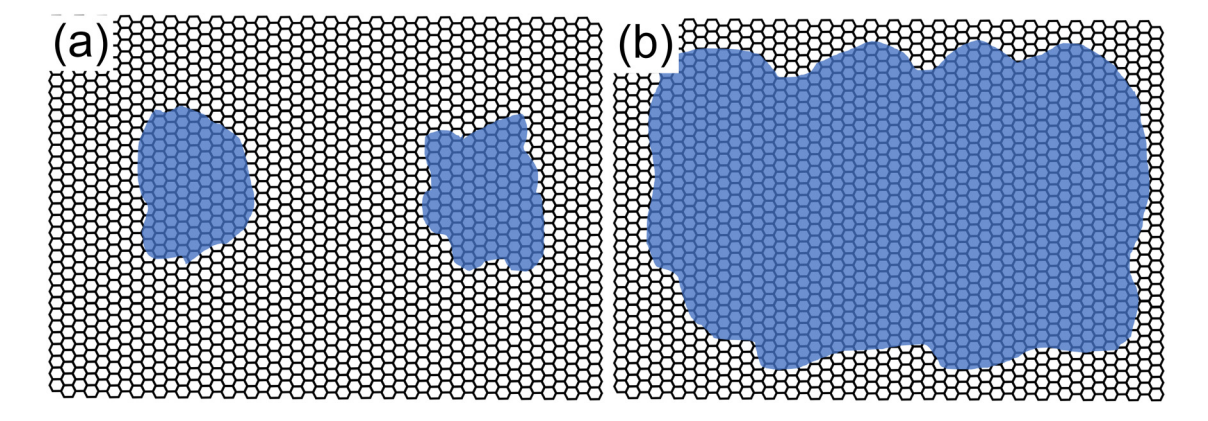


FIG. 3. Schematic of model. Shaded regions represent adsorbed water layers. (a) ML with low average water density. (b) ML with high average water density. Only areas covered by water become defective during irradiation.

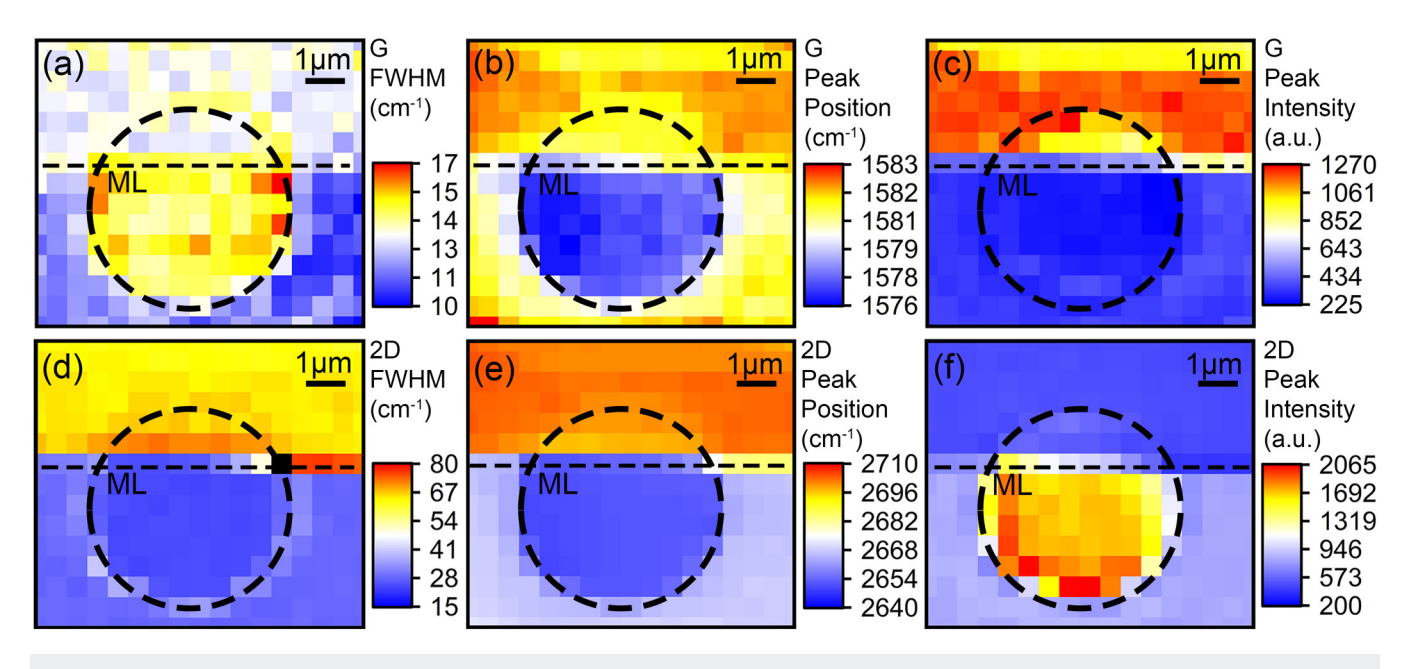


FIG. 4. Raman maps of the completely covered drum before irradiation. Dashed lines denote the boundaries between the hole and substrate, and ML and multilayer regions. (a)–(c) Maps of the FWHM, position, and height of the G peak, respectively. (d)–(f) Maps of the FWHM, position, and height of the 2D peak, respectively.

before irradiation are consistent with previous reports.<sup>32</sup> These reports state that the FWHM of the 2D peak of a pristine suspended ML is 2-6 cm<sup>-1</sup> less than that of the supported ML; we observe an average decrease in FWHM of 3.8 cm<sup>-1</sup>. We find an average increase in the position of the G peak of the suspended ML of 3.8 cm<sup>-1</sup>, from 1577.2 cm<sup>-1</sup> to 1581.0 cm<sup>-1</sup> for the supported ML. The position of the G peak is sensitive to strain with a coefficient of 10-15 cm<sup>-1</sup>/% strain, indicating little strain in our suspended ML. The 2D peak position for the suspended ML decreases by  $15.5 \text{ cm}^{-1}$  from  $2667.2 \text{ cm}^{-1}$  to  $2651.7 \text{ cm}^{-1}$ , consistent with earlier reports.<sup>32</sup> In Fig. 4(c), the intensity  $I_G$  in the supported ML is about a factor of 1.3 greater than that of the supported ML, 356 versus 274 a.u. This observation is also consistent with previous reports that explain this effect by multiple reflections in the drum and optical interference effects between the SiO<sub>2</sub> and the ML.<sup>32</sup> In contrast, the height of the 2D peak,  $I_{2D}$ , in the suspended ML in Fig. 4(f) is higher than that of the supported ML by a factor of 2.1. This effect is consistent with previous reports and is due to charged impurities in the SiO<sub>2</sub> that decrease the height of the 2D peak in the supported ML.

Figures 5(a)-5(f) show Raman maps of the G and 2D peaks of the completely covered drum after irradiation. The step size is  $0.2\,\mu\text{m}$ . The average changes in peak parameters in the suspended versus supported ML regions are more pronounced than in the nonirradiated sample. The average increase in FWHM of the G peak in the suspended ML versus the supported ML is about  $13.7\,\text{cm}^{-1}$  compared to  $2\,\text{cm}^{-1}$  for the nonirradiated ML; we attribute this to a high defect density in the suspended ML after irradiation. The position of the G peak of the suspended ML decreases by  $7.3\,\text{cm}^{-1}$  from its value in the supported ML, three times more

than in the nonirradiated sample. Therefore, the suspended ML may have more strain after irradiation. The intensity  $I_G$  of the suspended ML increases by a factor of 1.1 from its value in the supported ML, from 128 to 141 a.u., compared to a factor of 1.3 decrease for the nonirradiated sample. If the decrease in the nonirradiated case is due to optical effects, the increase after irradiation may also be due to optical effects, such as changes in the thickness or index of refraction of the ML after irradiation. For the 2D peak, the difference in peak position between the suspended and supported MLs is  $17.1 \, \mathrm{cm}^{-1}$ , similar to the nonirradiated ML. However,  $I_{2D}$  decreases by a factor of 1.2 from its value for the supported ML instead of increasing by a factor of 2.1, as seen in the nonirradiated ML. Since  $I_{2D}$  in the nonirradiated ML falls due to charged impurities in the substrate,  $^{32}$  the results after irradiation may be due to trapped charges in the defects in the suspended ML that may have a similar effect on the 2D peak.

Figures 6(a)-6(f) show Raman maps of the completely covered drum's D and D' peaks after irradiation. Similar to the D peak, the D' peak is defect activated except it involves intra- instead of intervalley scattering and LO instead of TO phonons. The step size of the maps is  $0.2\,\mu\text{m}$ . The black squares in the maps denote locations, where the software did not reliably fit the peaks due to their low heights. The D peak height is not sufficiently high in the supported multilayer region. However, it is higher and fittable in the suspended multilayer region. The D' peak is also not high enough in the supported multilayer and parts of the suspended multilayer region. The average increase in FWHM of the D peak in the suspended ML versus the supported ML is only  $2.9\,\text{cm}^{-1}$  from 18.7 to  $21.6\,\text{cm}^{-1}$ . These values are significantly smaller than those observed in Ar-irradiated graphene at high dosages and amorphous

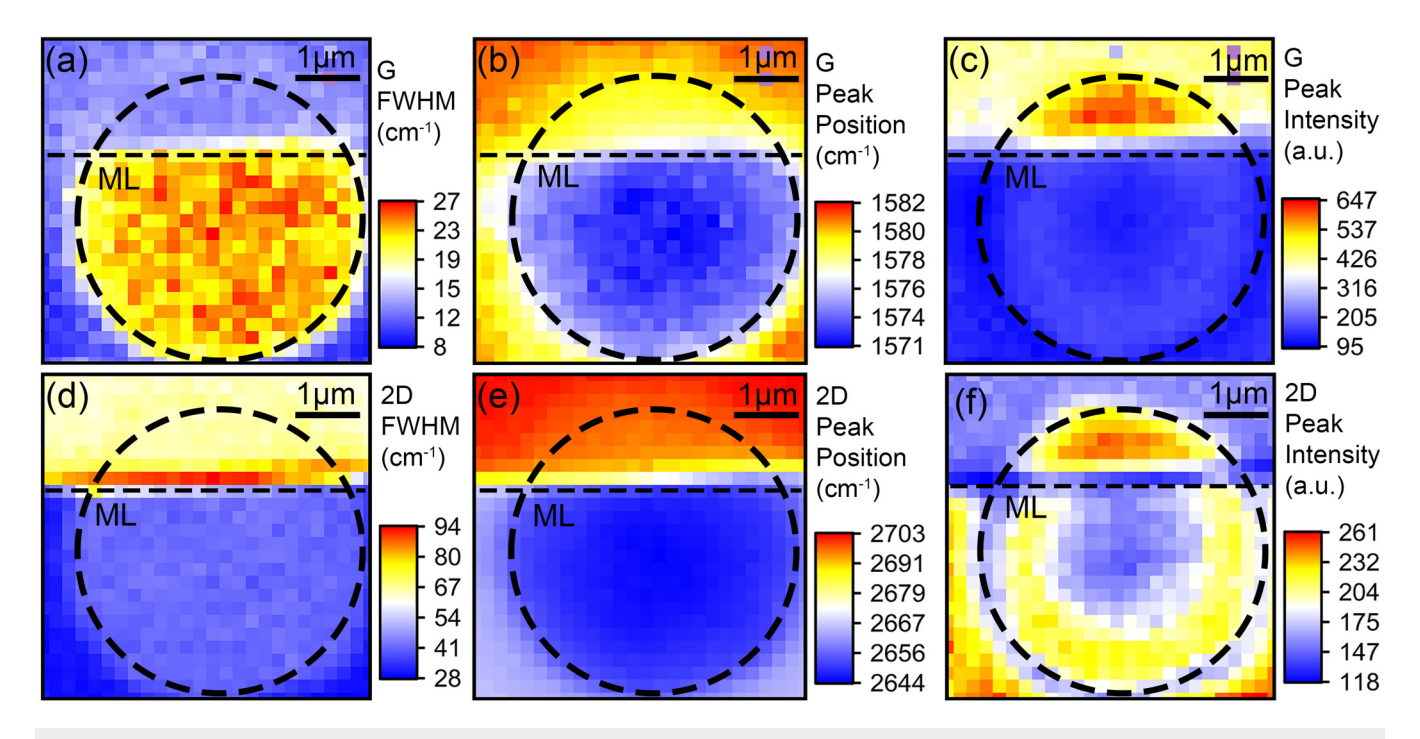


FIG. 5. Raman maps of the completely covered drum after irradiation. (a)–(c) Maps of the FWHM, position, and height of the G peak, respectively. (d)–(f) Maps of the FWHM, position, and height of the 2D peak, respectively.

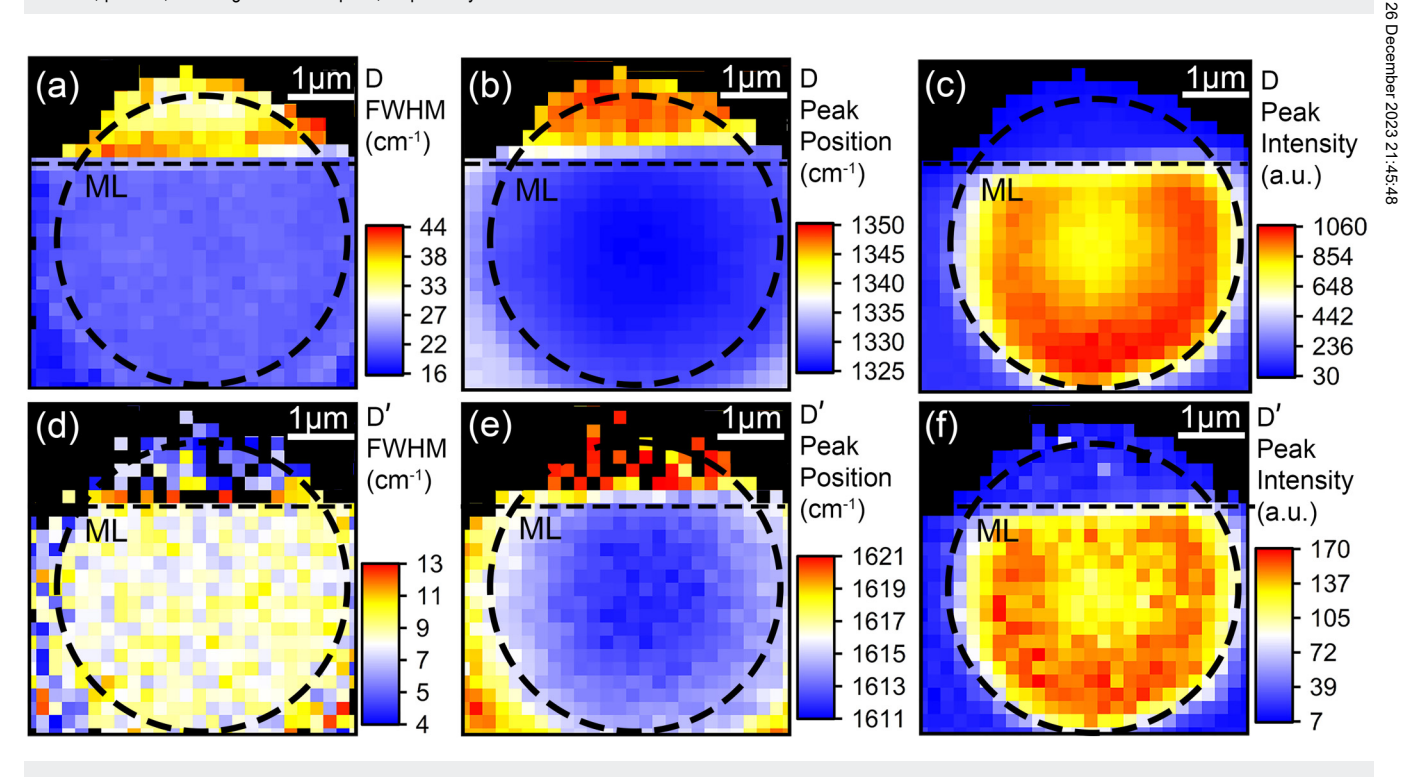
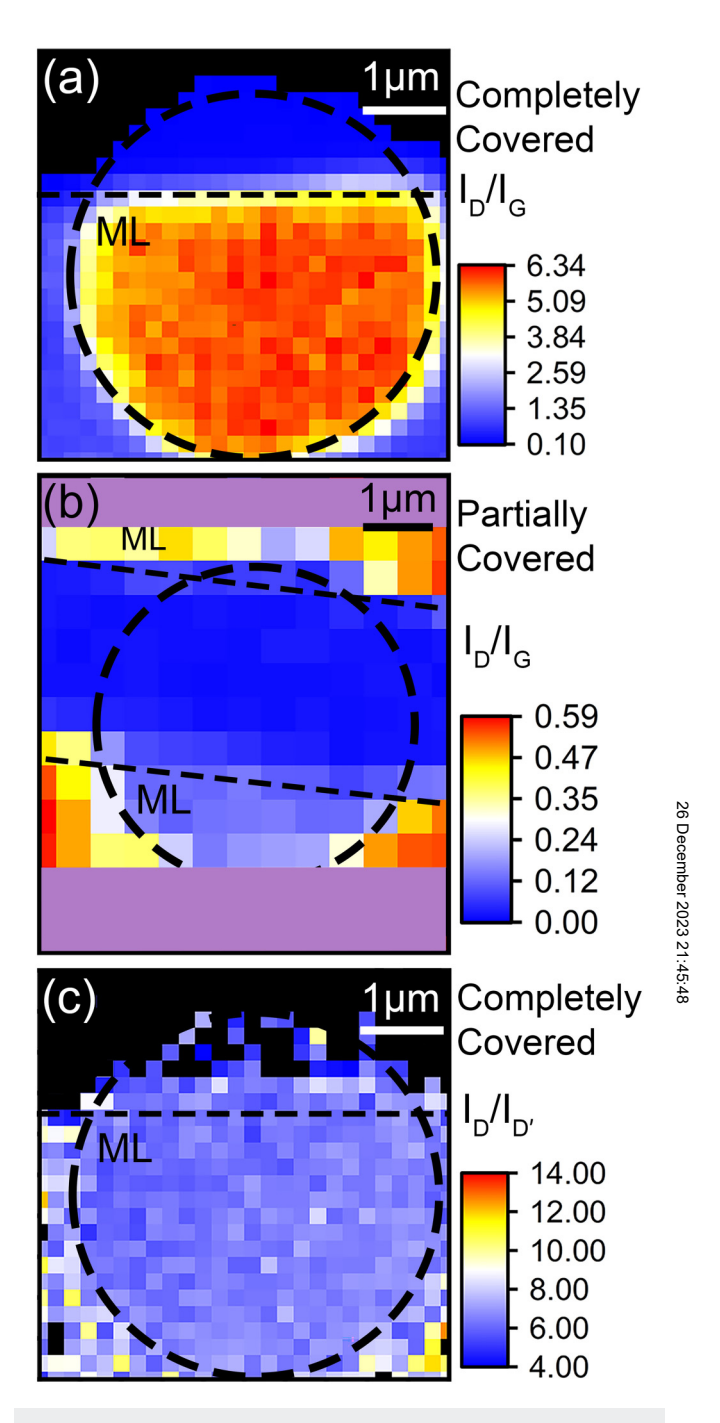


FIG. 6. Raman maps of the completely covered drum after irradiation. (a)–(c) Maps of the FWHM, position, and height of the D peak, respectively. (d)–(f) Maps of the FWHM, position, and height of the D' peak, respectively.

graphene, in which the FWHM of the D peak increases to about  $50~\rm cm^{-1}$ , indicating that the graphene lattice after irradiation, in our case, is less damaged. The position of the D peak of the suspended ML decreases by  $7.6~\rm cm^{-1}$  from its value in the supported ML. The intensity  $I_D$  in the suspended ML increases by over a factor of 30 from its value in the supported ML due to the high n in the supported ML. For the D peak, the difference in FWHM and peak position between the suspended and supported MLs is 0.5 and  $5.6~\rm cm^{-1}$ , respectively. We note that the intensities of the D, D, G, and 2D peaks in Figs. 5 and 6 show a ringlike structure around the perimeter of the hole that we believe is an optical effect due to multiple reflections in the hole since the corresponding maps of  $I_D/I_G$  and  $I_D/I_D$ , discussed below, do not show this structure.

Figures S4(a)-(i) in the supplementary material<sup>38</sup> show the features of the Raman peaks for the partially covered drum after irradiation. The FWHM of the G peak of the partially covered drum after irradiation is closer to that of the completely covered drum before irradiation than the completely covered drum after irradiation. The average FWHM of the G peak for the partially covered drum after irradiation, completely covered drum before irradiation, and completely covered drum after irradiation are 14.6, 14.8, and 23.7 cm<sup>-1</sup>, respectively; the FWHM of the 2D peaks are 23.3, 24.4, and 40.7 cm<sup>-1</sup>, respectively. Since the broadening of the G peak is an indicator of defects and disorder in the graphene lattice, 8-10,12 the significant broadening of the completely covered drum and less broadening of the partially covered drum supports our conclusion that adsorbates on the graphene present before irradiation play a considerable role in defect formation. The G and 2D peak positions for the partially covered and completely covered drums after irradiation shift in opposite directions. Since the positions of these peaks are sensitive to strain, the difference in shifts may be due to structural differences in the curvatures of the two drums due to different pressures in the drums. The G peak positions for the partially covered drum after irradiation, completely covered drum before irradiation, and completely covered drum after irradiation are 1581, 1577, and 1572 cm<sup>-1</sup>, respectively, and the 2D peak positions are 2666, 2652, and 2646 cm<sup>-1</sup>, respectively. The FWHM of the D peaks for the partially and completely covered drums are 14.0 and 21.6 cm<sup>-1</sup>, respectively, and the positions of the D peaks are 1337 and 1326 cm<sup>-1</sup>, respectively. The D peak of the completely covered drum is significantly broader and more shifted, which we attribute to a higher defect density.

Figures 7(a) and 7(b) show maps of  $I_D/I_G$  for the completely covered and partially covered drums, respectively, after irradiation obtained from the maps shown previously. The ringlike structure seen in the previous maps is not apparent. From Fig. 7(a), the average values of  $I_D/I_G$  for the suspended and supported MLs over and next to the completely covered drum are 5.90 and 0.94, respectively. The  $I_D/I_G$  values of the suspended ML range from 5.28 to 6.34, with a standard deviation of 0.34 or about 6% of the mean. As discussed previously, we attribute the significantly higher value for the suspended ML to a high adsorbed water density before irradiation. From Fig. 7(b), the average values of  $I_D/I_G$  for the suspended and supported MLs for the partially covered drum are 0.14 and 0.50, respectively.  $I_D/I_G$  is smaller for the suspended ML than the supported ML in this case. We attribute this to the partially covered drum having a low adsorbed water density on the ML



**FIG. 7.** (a) and (b) Maps of  $I_D/I_G$  for the completely and partially covered drums, respectively, after irradiation. (c) Map of  $I_D/I_D$  for the completely covered drum.

before irradiation; the supported ML retains adsorbed water between the ML and the substrate.

Figure 7(c) shows  $I_D/I_{D'}$  for the completely covered drum after irradiation. The average  $I_D/I_{D'}$  values for the suspended and

supported MLs are 6.87 and 8.17, respectively. Empirical studies on supported graphene and graphite show that the  $I_D/I_{D'}$  ratio in the first stage of defect formation indicates the nature of the defects. <sup>29,33,34</sup> The  $I_D/I_D$  ratio is ~8–13 for  $sp^3$ -type defects and ~5– 7 for vacancies. The explanation given for this is that the heights of both the D and D' peaks are proportional to n with different proportionality constants that depend on the nature of the defects but not on n, i.e.,  $I_D \sim An$  and  $I_D \sim Bn$ , where A and B are the proportionality constants. The empirical data imply that the defects in the suspended ML may be vacancies, while those on the supported ML  $sp^3$ -type defects. We will discuss this in more detail below.

Figures 8(a) and 8(b) show Raman spectra of the ML region over the completely covered drum and on the SiO2 substrate, respectively, after annealing. The annealing was done about a week after the irradiation was done. The spectra are averages of three spectra taken at the locations indicated in Fig. S5 in the supplementary material.<sup>38</sup> As shown in Fig. 8(a) for the completely covered drum, with increasing temperature from 25 to 215 °C, the  $I_D/I_G$  ratio decreases from 5.15 to 0.42. The significant decrease in  $I_D/I_G$  we observe at 215 °C is similar to that reported for hydrogenated graphene; for example, in Ref. 6, hydrogenated graphene's  $I_D/I_G$  ratio was about 0.5 after annealing at 200 °C. We observe  $I_D/I_G = 0.42$  after annealing at 215 °C. As shown in Fig. 8(a), the  $I_D/I_G$  ratio increases after annealing at 110 °C instead of decreasing, as expected if the suspended ML were in the first stage of defect formation. The increase

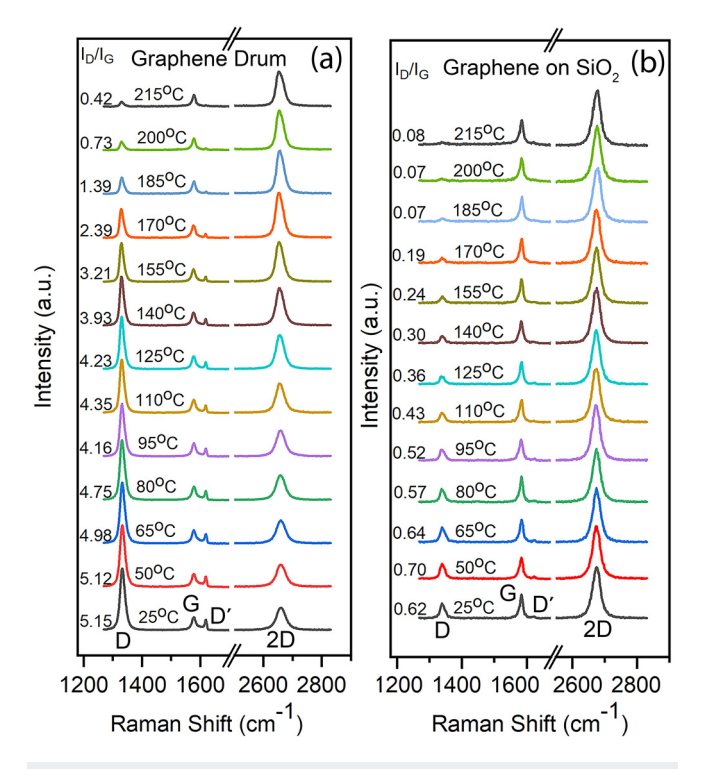


FIG. 8. Raman spectra after annealing at the specified temperatures. Shown are the resulting  $I_{\mathcal{D}}/I_{\mathcal{G}}$  ratios. (a) For the ML region over the completely covered drum. (b) For the ML region supported on the SiO<sub>2</sub> substrate.

may be due to parts of the suspended ML being in stage 2 where  $n \propto 1/(I_D/I_G)$ ; a decrease in n would increase  $I_D/I_G$ .

We analyze the annealing data in Fig. 8 using an Arrhenius plot. We utilize a bimodal rate equation

$$dn/dt = -Cn^2 e^{-\frac{E_a}{k_B T}}.$$

Here, C is a constant, T is the annealing temperature in degrees Kelvin,  $E_a$  is the activation energy for defect healing, and  $k_B$  is the Boltzmann constant. A bimodal equation is consistent with reactions involving two similar entities, exemplified by hydrogen desorption by the recombination of two adsorbed hydrogen atoms and graphene vacancy healing.<sup>35</sup> Integrating over an annealing period  $\Delta t = t_2 - t_1$ , where the subscripts denote subsequent anneals, yields the relation  $1/n_2 - 1/n_1 = \hat{\Delta t} C e^{-E_a/k_B T}$ . Utilizing the approximation that  $n \propto I_D/I_G$  results in this relation becoming  $\ln [(I_G/I_D)_2 - (I_G/I_D)_1] = \ln (\Delta t) + \ln (C) - E_a/k_BT$ . As shown in Fig. 8(a), for the completely covered drum, the Raman spectra obtained after the 110 and 125 °C anneals result in negative values for the argument of the natural logarithm and so are omitted. As shown in Fig. 8(b), for the supported ML region, the Raman spectra after the 50 and 65 °C anneals result in negative arguments of the natural logarithm and are omitted. Figure 9(a) shows plots of the experimental data (solid circles) and a least-squares fit (solid

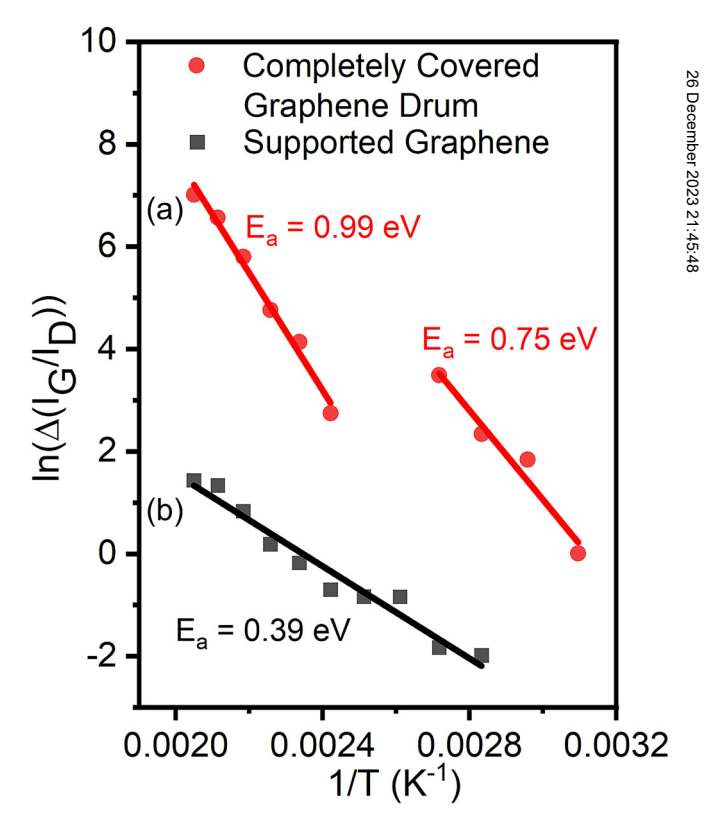
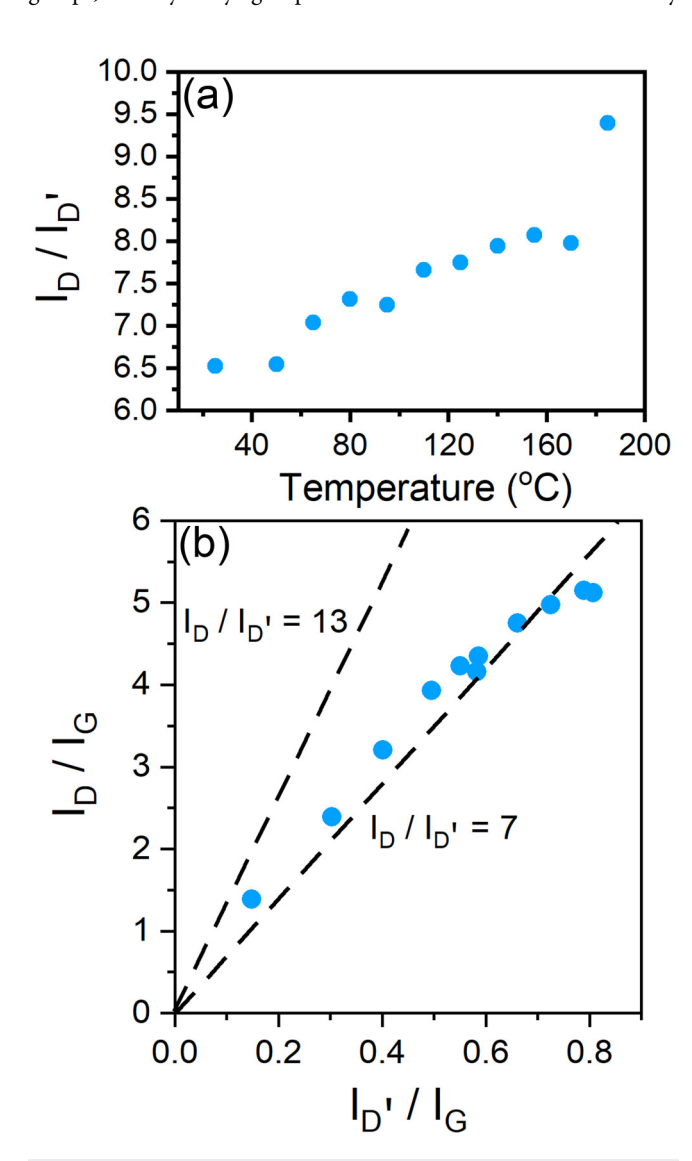


FIG. 9. Arrhenius plot of the annealing data. (a) The suspended ML over the completely covered drum. (b) Supported ML.

line) to the data for the completely covered drum using the above equation. As shown in Fig. 9(a), there are two linear regions with different slopes. We obtain two activation energies of  $E_a = 0.75 \text{ eV}$ and  $E_a = 0.99$  eV from the slopes. Figure 9(b) shows a plot of the data and least-squares fit for the supported ML, from which we obtain an activation of  $E_a = 0.39$  eV. This value is similar to  $E_a = 0.48 \text{ eV}$  that we previously reported for supported ML graphene in the second stage. Calculations of migration barriers of single hydrogen atoms, hydroxyl groups, and hydroxyl groups with attached water molecules on graphene show that the migration barriers depend on the distance between adsorbates.<sup>36</sup> As a function of distances from 0.75 to 2.0 nm, the barriers for hydrogen, hydroxyl groups, and hydroxyl groups with attached water molecules vary



**FIG. 10.** (a)  $I_D/I_{D'}$  of the spectra in Fig. 5 as a function of annealing temperature. (b) Plot of  $I_D/I_G$  vs  $I_D/I_G$  from the spectra in Fig. 5.

from about 1.0 to 0.3, 0.5 to 1.0 eV, and 0.7 to 0.6 eV, respectively.<sup>36</sup> Since we estimated  $L_D = 2.5$  nm in our case, the distance between adsorbates is at the long-distance limit, and the migration barriers for hydrogen, hydroxyl groups, and hydroxyl groups with attached water molecules would be about 0.3, 1.0, and 0.6 eV, respectively. In addition, calculations show that stress can significantly increase migration barriers.<sup>37</sup> For the supported ML,  $E_a$  is closest to the migration barrier for hydrogen. For the suspended ML, the two values of  $E_a$  are most comparable to hydroxyl groups and hydroxyl groups with attached water molecules. For the suspended ML, vacancies, which have an activation energy for healing of 0.95 eV, are possible.

We also studied the effects of annealing on the  $I_D/I_{D'}$  ratio. As previously discussed, it has been reported that in the first stage  $I_D/I_{D'} \sim A/B$ , where A and B are constants independent of the defect density n. Figure 10(a) shows  $I_D/I_{D'}$  of the suspended ML as a function of annealing temperature up to 185 °C. At higher temperatures, we could not reliably fit the D' peak. As the annealing temperature increases, we expect that n will decrease since the defects start to heal. As shown in Fig. 10(a), the  $I_D/I_{D'}$  ratio increases with annealing temperature, appearing to depend on n. The  $I_D/I_{D'}$  ratio is about 8 after annealing at 140 °C and increases to about 9.4 after annealing at 185 °C. Figure 10(b) shows the data plotted  $I_D/I_G$  versus  $I_D/I_G$  and lines with slopes corresponding to  $I_D/I_{D'} = 13$  and 7. As the  $I_D/I_G$  ratio decreases,  $I_D/I_{D'}$  increases. Figure S6 in the supplementary material<sup>38</sup> shows that after annealing at 215 °C the  $I_D/I_G$  ratio is 0.42, but the D' peak is not observable within the noise. Assuming  $I_{D'}$  is at the standard deviation of  $\frac{8}{2}$ the noise, the  $I_D/I_D$  ratio would be greater than 13. We hypothesize that the apparent dependence of  $I_D/I_D$  on n for the suspended ML is contact to the apparent of the formula and ML is a functional data from the suspended ML. in contrast to the empirical data for supported MLs is due to parts of the supported ML being in the second stage of defect formation or substrate interactions. Since the suspended ML is isolated from the substrate, it may be more sensitive to changes in n.

#### IV. SUMMARY AND CONCLUSIONS

In summary, we have used an SEM to irradiate graphene drums with electrons having an energy of 20 keV to a dosage of about  $1.58 \times 10^{17}$  electrons/cm<sup>2</sup>. We found that after irradiation, suspended graphene MLs over completely covered holes have a value of  $I_D/I_G$  as high as 6.3, significantly higher than the maximum  $I_D/I_G$  of about 3.3 previously reported for supported ML graphene exposed to electron irradiation, hydrogen plasma, and Ar ion bombardment. We studied the effects of the irradiation using Raman spectroscopy maps. After irradiation, we found that the  $I_D$ / I<sub>G</sub> ratio was uniform across the suspended ML region, with a standard deviation of about 6% of the mean. We studied the nature of the defects by annealing the sample. We found a significant decrease in  $I_D/I_G$  as the annealing temperature increased from 50 to 215 °C. We obtained an Arrhenius plot from the annealing data and found activation energies for healing of  $E_a = 0.7$  and 0.99 eV for the suspended ML and  $E_a = 0.39$  eV for the supported ML. The values for the suspended ML are close to migration barriers for hydroxyl groups (1.0 eV), vacancies (0.95 eV), and hydroxyl groups with attached water molecules (0.6 eV). The value for the supported ML is close to the migration barrier of hydrogen (0.3 eV).

We also studied the  $I_D/I_{D'}$  ratio and found it before annealing to have average values of 6.87 and 8.17 for the suspended and supported ML, respectively. Empirical studies have shown that for supported graphene and graphite in the first stage, the  $I_D/I_D$  ratio is about 8-13 for sp<sup>3</sup> defects such as adsorbates and 5-7 for vacancies, implying that the defects in the suspended ML after annealing may be vacancies. However, we studied the temperature dependence of the  $I_D/I_{D'}$  ratio in the suspended ML and found that it appears to depend on n. The  $I_D/I_{D'}$  ratio increases with decreasing  $I_D/I_G$ , approaching values of about 8 and greater for  $I_D/I_G$  ratios less than about 3.9. Our results show that electron irradiation of graphene drums may be helpful for modifying graphene with defects at high average densities.

# **ACKNOWLEDGMENTS**

We thank Wonbong Choi and Pashupati Adhikari for their contributions to this project. This work was performed in part at the University of North Texas's Materials Research Facility: A shared research facility for multidimensional fabrication and characterization. This material is based upon work supported by the National Science Foundation (NSF) under Grant No. DMR-2312436.

#### **AUTHOR DECLARATIONS**

#### Conflicts of Interest

The authors have no conflicts to disclose.

#### **Author Contributions**

Ibikunle Ojo: Data curation (lead); Formal analysis (lead); Methodology (lead); Validation (equal); Writing - original draft (equal); Writing - review & editing (lead). Evan Hathaway: Data curation (equal); Formal analysis (equal); Methodology (equal); Software (equal). Jianchao Li: Methodology (equal). Roberto Gonzalez: Data curation (equal); Formal analysis (equal); Methodology (equal). Yan Jiang: Formal analysis (equal); Methodology (equal); Validation (equal). Jingbiao Investigation (equal); Methodology (equal); Project administration (equal); Supervision (equal). Jose Perez: Conceptualization (lead); Data curation (equal); Formal analysis (equal); Funding acquisition (lead); Investigation (lead); Methodology (equal); Project administration (lead); Resources (equal); Software (equal); Supervision (lead); Validation (equal); Visualization (equal); Writing - original draft (equal); Writing - review & editing (equal).

# DATA AVAILABILITY

The data that support the findings of this study are available from the corresponding author upon reasonable request.

#### REFERENCES

- <sup>1</sup>D. Teweldebrhan and A. A. Balandin, Appl. Phys. Lett. 94, 013101 (2009).
- <sup>2</sup>M. Z. Iqbal, O. Kelekci, M. W. Iqbal, and J. Eom, Carbon **59**, 366 (2013).
- <sup>3</sup>I. Childres, L. A. Jauregui, W. Park, H. Cao, and Y. P. Chen, New Developments in Photon and Materials Research (Nova Science Publishers, New York, 2013).
- <sup>4</sup>A. E. Islam et al., Carbon 166, 446 (2020).

- <sup>5</sup>I. A. Ojo et al., J. Vac. Sci. Technol. A **41**, 012201 (2022).
- 6S. Ryu, M. Y. Han, J. Maultzsch, T. F. Heinz, P. Kim, M. L. Steigerwald, and L. E. Brus, Nano Lett. 8, 4597 (2008).
- 7F. Zhao, Y. Raitses, X. Yang, A. Tan, and C. G. Tully, Carbon 177, 244
- <sup>8</sup>E. H. M. Ferreira, M. V. O. Moutinho, F. Stavale, M. M. Lucchese, R. B. Capaz, C. A. Achete, and A. Jorio, Phys. Rev. B 82, 125429 (2010).
- <sup>9</sup>M. M. Lucchese, F. Stavale, E. H. M. Ferreira, C. Vilani, M. V. O. Moutinho, R. B. Capaz, C. A. Achete, and A. Jorio, Carbon 48, 1592 (2010).
- 10 L. G. Cançado et al., Nano Lett. 11, 3190 (2011).
- 11 J. S. Bunch, S. S. Verbridge, J. S. Alden, A. M. Van Der Zande, J. M. Parpia, H. G. Craighead, and P. L. McEuen, Nano Lett. 8, 2458 (2008).
- <sup>12</sup>A. C. Ferrari and J. Robertson, Phys. Rev. B **61**, 14095 (2000).
- <sup>13</sup>F. Banhart, Rep. Prog. Phys. **162**, 1181 (1999).
- <sup>14</sup>J. C. Meyer et al., Phys. Rev. Lett. **108**, 196102 (2012).
- 15Y. Zhou, J. Jadwiszcak, D. Keane, Y. Chen, D. Yu, and H. Zhang, Nanoscale 9,
- 16 F. Withers, T. H. Bointon, M. Dubois, S. Russo, and M. F. Craciun, Nano Lett. 11, 3912 (2011).
- 17W. K. Lee, K. E. Whitener, J. T. Robinson, and P. E. Sheehan, Adv. Mater. 27, 1774 (2015).
- <sup>18</sup>J. D. Jones, K. K. Mahajan, W. H. Williams, P. A. Ecton, Y. Mo, and J. M. Perez, Carbon 48, 2335 (2010).
- <sup>19</sup>S. J. Cartamil-Bueno, P. G. Steeneken, A. Centeno, A. Zurutuza, H. S. van der Zant, and S. Houri, Nano Lett. 16, 6792 (2016).
- <sup>20</sup>P. Yin and M. Ma, ACS Appl. Nano Mat. 1, 6596 (2018).
- 21 Y. Manzanares-Negro, P. Ares, M. Jaafar, G. López-Polín, C. Gómez-Navarro, and J. Gómez-Herrero, Appl. Mater. Interfaces 12, 37750 (2020).
- <sup>22</sup>M. Lee, D. Davidovikj, B. Sajadi, M. Šiškins, F. Alijani, H. S. Van Der Zant, and P. G. Steeneken, Nano Lett. 19, 5313 (2019).
- <sup>23</sup>P. Z. Sun et al., Nature **579**, 229 (2020).
- r. L. Sun et al., Nature 5/9, 229 (2020).

  24S. P. Koenig, N. G. Boddeti, M. L. Dunn, and J. S. Bunch, Nat. Nanotechnol. 6, 543 (2011).

  25I. E. Rosłoń, A. Japaridze, P. G. Steeneken, C. Dekker, and F. Alijani, Nat. Nanotechnol. 17, 637 (2022).

  26M. Šiškins et al., Microsyst. Nanoeng. 6, 102 (2020).

  27Q. Wang, W. Hong, and L. Dong, Nanoscale 8, 7663 (2016).

  28A. F. Carvalho, B. Kulyk, A. J. Fernandes, E. Fortunato, and F. N. Costa, Adv. Mater. 34, 2101336 (2022).

- Mater. 34, 2101326 (2022).
- 29 R. Selhorst, M. A. Susner, R. Muzzio, I. H. Kao, J. Carpena-Núñez, A. E. Islam, J. Katoch, B. Maruyama, and R. Rao, Vacuum 207, 111686
- 30 A. Akaishi, T. Yonemaru, and J. Nakamura, ACS Omega 2, 2184 (2017).
- 31 C. Melios, C. E. Giusca, V. Panchal, and O. Kazakova, 2D Mater. 5, 0220
- 32Z. H. Ni, T. Yu, Z. Q. Luo, Y. Y. Wang, L. Liu, C. P. Wong, J. Miao, W. Huang, and Z. X. Shen, ACS Nano 3, 569 (2009).
- 33A. Eckmann, A. Felten, A. Mishchenko, L. Britnell, R. Krupke, K. S. Novoselov, and C. Casiraghi, Nano Lett. 12, 3925 (2012).
- 34J. Jiang, R. Pachter, F. Mehmood, A. E. Islam, B. Maruyama, and J. J. Boeckl, Carbon 90, 53 (2015).
- 35 J. Chen, T. Shi, T. Cai, T. Xu, L. Sun, X. Wu, and D. Yu, Appl. Phys. Lett. 102, 103107 (2013).
- <sup>36</sup>D. W. Boukhvalov, Phys. Chem. Chem. Phys. **12**, 15367 (2010).
- 37H. McKay, D. J. Wales, S. J. Jenkins, J. A. Verges, and P. L. De Andres, Phys. Rev. B 81, 075425 (2010).
- 38 See supplementary material online for a description of Raman maps of the partially covered drum after irradiation, locations where the Raman spectra for the annealing studies were averaged, and the Raman spectrum of the D' peak after annealing at 215 °C.